

www.acsnano.org

Singular and Nonsingular Transitions in the Infrared Plasmons of Nearly Touching **Nanocube Dimers**

Yina Wu, Andrea Konečná, Shin Hum Cho, Delia J. Milliron, Jordan A. Hachtel,* and F. Javier García de Abajo*



Downloaded via UNIV OF TEXAS AT AUSTIN on June 12, 2024 at 13:12:23 (UTC). See https://pubs.acs.org/sharingguidelines for options on how to legitimately share published articles.

Cite This: ACS Nano 2024, 18, 15130-15138



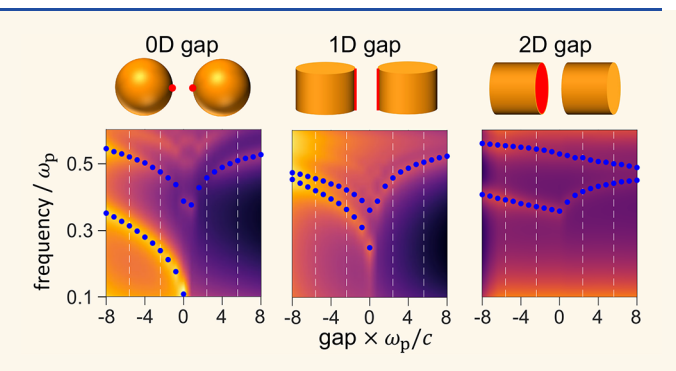
ACCESS I

Metrics & More

Article Recommendations

Supporting Information

ABSTRACT: Narrow gaps between plasmon-supporting materials can confine infrared electromagnetic energy at the nanoscale, thus enabling applications in areas such as optical sensing. However, in nanoparticle dimers, the nature of the transition between touching (zero gap) and nearly nontouching (nonzero gap ≤15 nm) regimes is still a subject of debate. Here, we observe both singular and nonsingular transitions in infrared plasmons confined to dimers of fluorine-doped indium oxide nanocubes when moving from touching to nontouching configurations depending on the dimensionality of the contact region. Through spatially resolved electron energy-loss spectroscopy, we find a continuous spectral evolution of the lowest-



order plasmon mode across the transition for finite touching areas, in excellent agreement with the simulations. This behavior challenges the widely accepted idea that a singular transition always emerges in the near-touching regime of plasmonic particle dimers. The apparent contradiction is resolved by theoretically examining different types of gap morphologies, revealing that the presence of a finite touching area renders the transition nonsingular, while one-dimensional and point-like contacts produce a singular behavior in which the lowest-order dipolar mode in the touching configuration, characterized by a net induced charge in each of the particles, becomes unphysical as soon as they are separated. Our results provide valuable insights into the nature of dimer plasmons in highly doped semiconductors.

KEYWORDS: infrared plasmons, nanodimers, fluorine-doped indium oxide, electron energy-loss spectroscopy (EELS), confined optical modes

Plasmons in metallic nanostructures have received considerable attention because they allow for the manipulation of light at the nanoscale. 1-6 In particular, plasmons confined to narrow gaps (in the few- or sub-nanometer range) between two metallic surfaces can yield extreme field amplification^{7–11} that enables applications in enhanced optical sensing, 12,13 photocatalysis, 14,15 and light harvesting, 16 among other feats. The spectral and spatial characteristics of gap plasmons can be accurately tuned by playing with the surface morphology, gap separation, and composition of the nanostructures. These types of confined optical modes have been studied in dimers formed by different types of particles, such as nanorods,²³ nanoshells, 24,25 and nanocubes. 26,27 At large separations compared to the particle sizes, the plasmons of individual nanoparticles having a net-induced dipole are hybridized due to their Coulombic interaction, in direct analogy to the formation of chemical bonding orbitals. ^{28,29} When the particles approach each other, more complex gap modes are observed,

composed of multipolar plasmons for small separations compared with the particle sizes.^{29,30} Eventually, when the particles touch and become a single sintered structure, a singular behavior can be observed, translated, for example, in the emergence of modes with a net induced charge in each of the particles, which were unphysical in the separate dimer. Singular behavior is therefore observed in the spectra as a discontinuity of the plasmon energies as a function of gap separation when we go from positive (nontouching particles) to negative (overlapping particles) values of this parameter.

Received: February 25, 2024 Revised: May 3, 2024 Accepted: May 9, 2024

Published: May 28, 2024





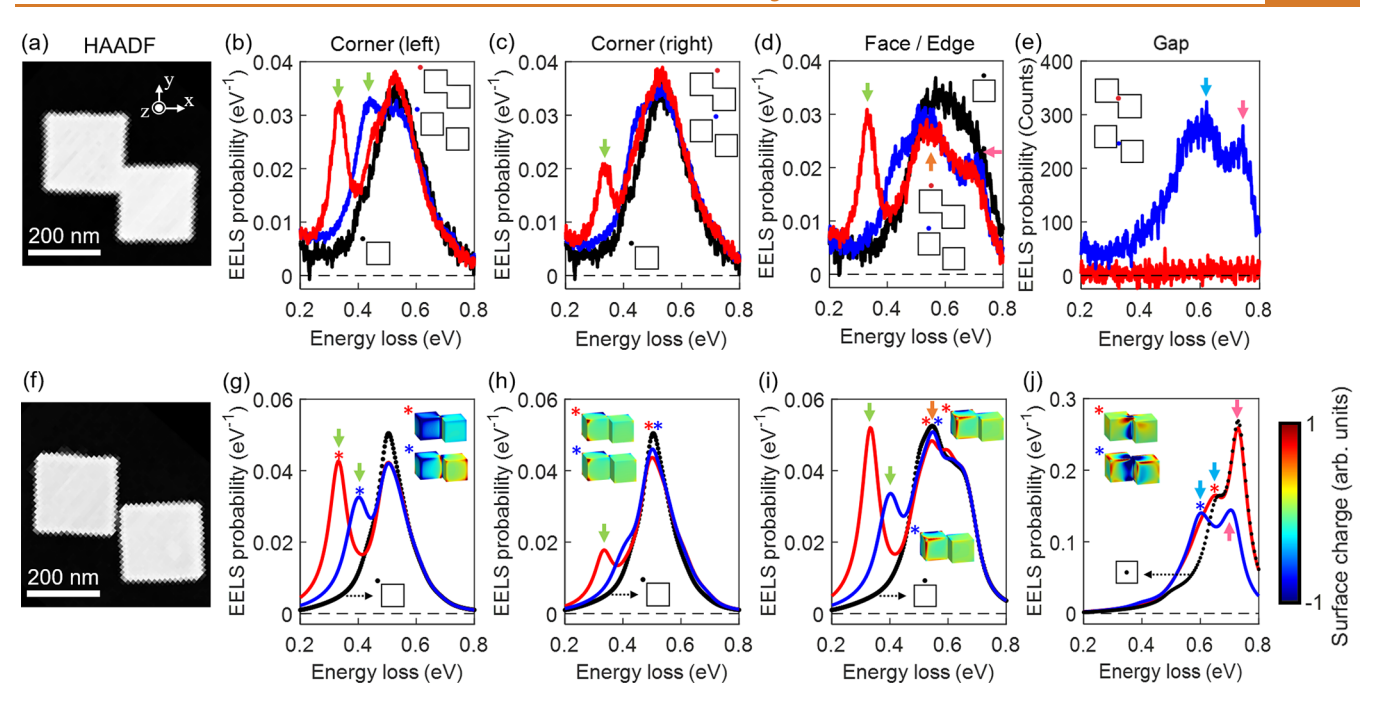


Figure 1. Infrared plasmons in touching and nontouching nanocube dimers. We show EELS measurements for e-beams aimed at different locations around touching and nontouching (\sim 10 nm gap) F-IO nanocubes of 200 nm side length. (a,f) High-angle annular dark-field (HAADF) micrographs showing touching (a) and nontouching (f) dimers. (b-e) EELS spectra measured in the samples of (a) at the positions indicated by the color-coordinated dots in the insets. (g-j) Simulated spectra corresponding to the configurations in (b-e), along with schematic charge distributions (see insets, in saturated color scale). Experiments and simulations for individual nanocubes are shown for comparison in (b-d) (black curves) and (g-j) (black-dotted curves), respectively. The electron moves along the z axis [see coordinate frame in (a)] with an energy of 60 keV.

The ensuing spectral discontinuities in the transition from touching to nontouching conditions have been reported for dimers formed by nanodisks, ³¹ nanorods, ³² and nanoshells, ²⁴ while they are quantitatively explained through dielectric theory for gold-sphere dimers, ²⁹ although electron tunneling in narrow gaps may play a role that has been a subject of debate ^{33,34} that we do not consider in the present work.

Noble metals such as gold and silver are commonly used as a playground to study plasmons, offering strong field confinement, mainly in the visible spectral range. In the infrared spectral region, high spatial confinement is commonly accompanied by strong losses limited by the intrinsic lifetime in the bulk metal. Oxides with high electrical conductivity and optical transparency, like tin- or fluorine-doped indium oxide (F-IO), 35,36 represent an alternative to more conventional infrared plasmonic materials. Typical carrier concentrations achievable via chemical doping or electrochemical reactions in F-IO naturally yield highly confined, low-energy plasmons whose energies can be tuned on demand.^{37–43} Moreover, the synthesis processes lead to well-defined particle morphologies, while upon deposition on a surface, dimers can be found in which the particles are either touching or separated by narrow gaps, thus providing a suitable platform to examine the infrared plasmonic response in the transition between these two regimes.

Here, we address the dramatic dependence of plasmons in the near-touching particle-dimer regime on the dimensionality of the touching region. Specifically, we analyze the singular character of the transition between touching and nontouching configurations of F-IO nanocubes synthesized in solution and deposited on a transmission electron microscopy (TEM) membrane. We perform electron energy-loss spectroscopy

(EELS) and observe dimer plasmons whose spectral and spatial characteristics are in excellent agreement with electromagnetic simulations, revealing the transition between touching and nontouching regimes and addressing the intriguing dependence on the dimensionality of the touching region. Specifically, the transition is observed to be singular when the touching region is either point-like or edge-like, which we analyze through numerical simulations for different particle morphologies, including cube pairs with an edge-toedge arrangement. This is in contrast to the smoother spectral evolution found in the plasmon modes in a face-to-face arrangement (i.e., for a finite contact area). Our experimental and theoretical results conclusively establish the relation between the dimensionality of the touching region and the singular character of the transition between touching and nontouching configurations in infrared plasmonic nanoparticles.

RESULTS AND DISCUSSION

Our starting point is the synthesis of F-IO nanocubes with 200 nm side lengths through colloid chemistry followed by their deposition on TEM silicon-nitride membranes of 25 nm thickness (see Methods). Upon inspection, we identified individual particles as well as touching and nontouching dimers. Analysis of the spectral and spatial characteristics of the plasmons supported by these samples is then performed through EELS in the scanning TEM mode. In particular, individual nanocubes exhibit familiar plasmon features in the spectra delated characterized by corner, face, and bulk modes (see Figures S1 and S2 in the Supporting Information), which are well reproduced by EELS theory (see Methods). We neglect the effect of the membrane, which complicates the numerical

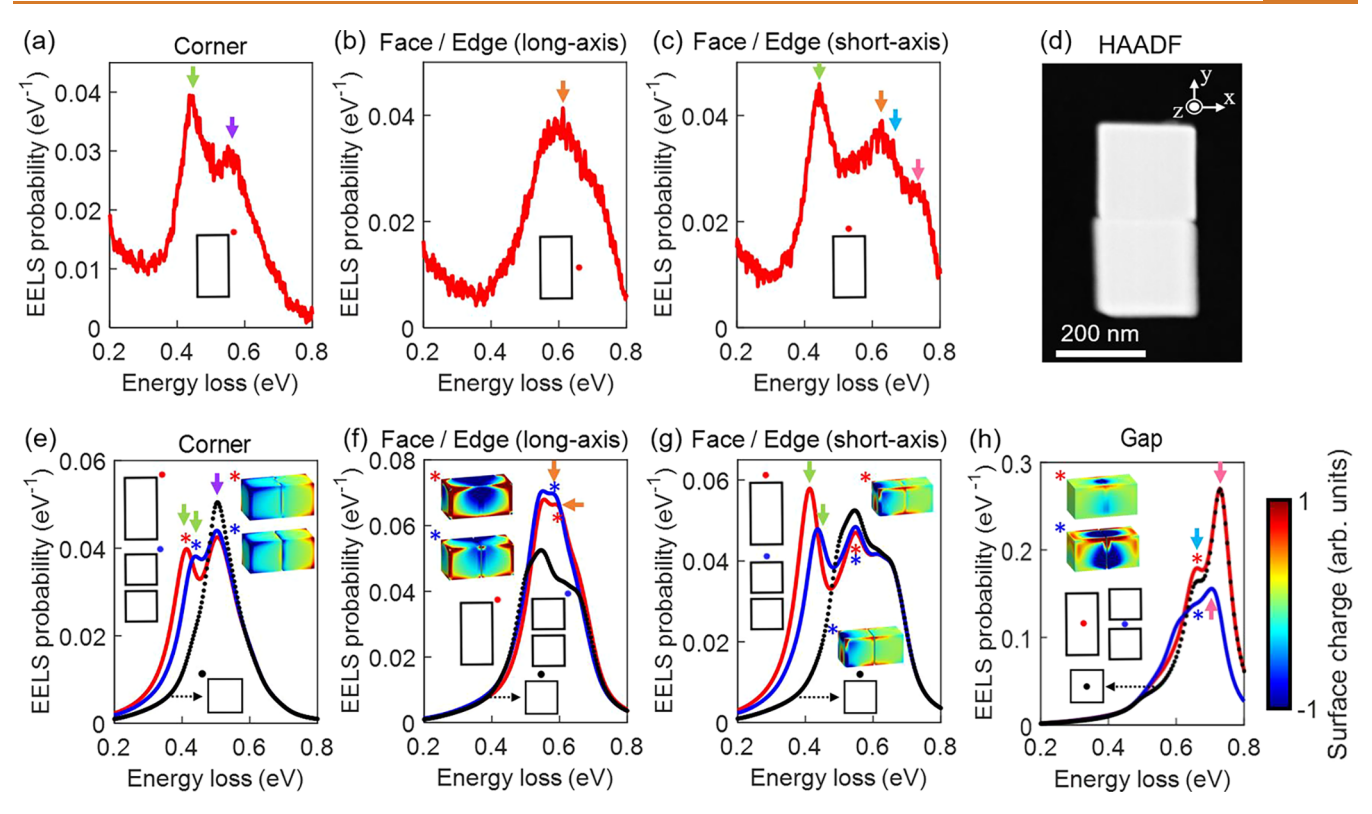


Figure 2. Infrared face-to-face dimer plasmons. We compare EELS measurements and calculations for e-beams aimed at different locations around face-to-face touching and nontouching dimers (\sim 10 nm gap) formed by F-IO nanocubes of 200 nm side length. (a–c) Measured EELS spectra at the three e-beam positions indicated by the red dots in the insets. The electron energy is 60 keV. (d) HAADF micrograph showing a face-to-face touching dimer. (e–g) Simulated spectra under the conditions of (a–c), along with 3D renderings of the electron-induced charge distributions at the frequencies of the dominant peaks in the spectra (insets, in saturated color scale), indicated by red and blue asterisks for touching and nontouching dimers, respectively. (h) Simulated spectra for an e-beam passing by the gap in the nontouching dimer and through the center in the touching dimer (see insets). In (e–h), we include spectra for an individual nanocube for comparison (black-dotted curves for beam positions denoted by black dots in the insets).

simulation while only adding minor redshifts (see Figure S16 in Supporting Information) because its thickness is small compared to the cube size and it does not support any excitations in the energy region of interest, apart from a broad band of very delocalized guided modes. In addition, we describe the F-IO material through a frequency-dependent local permittivity with the modified Drude form

$$\epsilon(\omega) = \epsilon_{\rm b} - \frac{\omega_{\rm p}^2}{\omega(\omega + i\gamma)}$$
(1)

where the background permittivity ϵ_b = 4 and the phenomenological damping $\hbar \gamma = 0.07$ eV are taken from previous studies, 35 while the Drude weight $\omega_{\rm p}$ is fitted to match the actual level of F doping in the samples. Excellent agreement with our measurements is obtained for $\hbar\omega_{\rm p}$ = 1.46 eV. Because the cubes are small compared to the light wavelength in the plasmonic spectral region, the observed mode energies of individual particles are in excellent agreement with electrostatic mode theory, 44 in which the plasmon frequencies ω_i are signaled by resonant values of the permittivity $\epsilon(\omega_i) = \epsilon_i$ (i.e., $\omega_i = \omega_p / \sqrt{\epsilon_b - \epsilon_i}$, if we neglect material losses). In particular, the theory predicts two strong corner and edge modes with a net dipolar moment at $\epsilon_1 \approx$ -3.68 and $\epsilon_2 \approx -2.37$ (i.e., $\hbar\omega_1 \approx 0.53$ eV and $\hbar\omega_2 \approx 0.58$ eV) in good agreement with the lowest-energy features in the spectra acquired under aloof electron-beam (e-beam) excitation (black curves in Figure 1, and more details in

Figure S1), as well as a weaker dipolar face mode at $\epsilon_3 \approx -0.78$ (i.e., $\hbar\omega_3 \approx 0.67$ eV), which also couples well to the electron. For penetrating trajectories, the bulk plasmon corresponding to $\epsilon_{\rm bulk} = 0$ emerges as a spectral feature at $\hbar\omega_{\rm bulk} \approx 0.73$ eV.

Examples of dimers found in our samples for touching and nontouching (~10 nm gap) configurations are shown in the dark-field images of Figure 1a,f. As shown in the measured spectra of Figure 1b-e, a salient difference between these two types of dimers is the presence of a low-energy plasmon (~0.33 eV spectral feature) for touching particles (red curves), which is not present for nontouching nanocubes (blue curves). This mode is more prominently excited when the e-beam is placed farther from the dimer center (Figure 1b,d). Together with other observed spectral features, these results are well reproduced by EELS simulations (Figure 1g-j), which also allow us to visualize the charge ordering associated with the different plasmon modes. In particular, the low-energy plasmon involves a net charge transfer between the two nanocubes, which is of course forbidden in the gapped dimer configuration, as previously analyzed in a study based on extensive electromagnetic simulations for gold-sphere dimers.²⁹ Apart from this dipolar mode, the rest of the plasmons are similar to those observed in individual nanocubes (black curves in Figure 1), although they undergo spectral shifts due to the interaction with the neighboring particle. Incidentally, when the e-beam is aimed at the dimer center (Figure 1e), the spectrum is depleted in the touching configuration as a result of strong scattering suffered by the

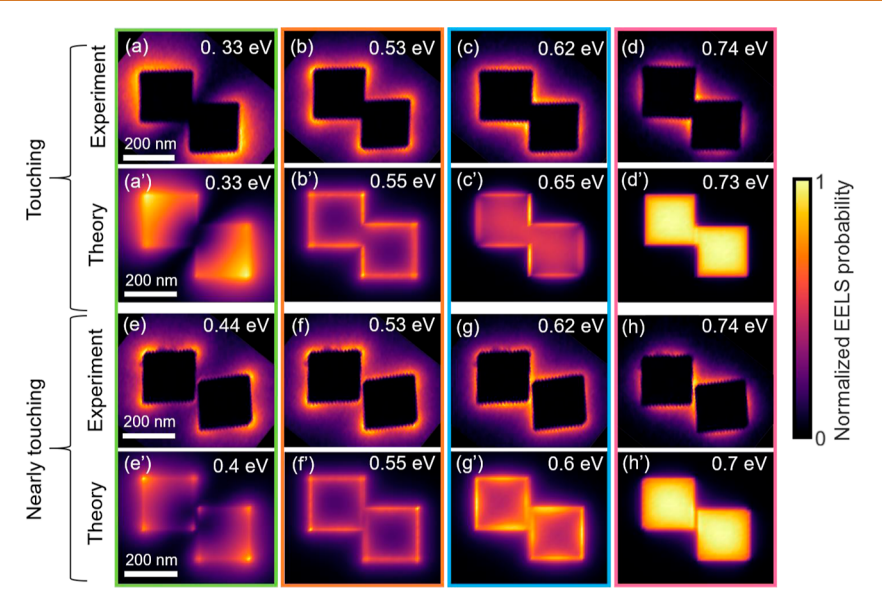


Figure 3. Energy-filtered EELS maps of the dominant plasmons in touching and nearly touching nanocube dimers. We show measured EELS maps at 60 keV electron energy for the same touching (a-d) and near-touching (e-h) dimers as in Figure 1, as well as the corresponding simulations (a'-d',e'-h'). Mode energies (see labels) are also indicated by arrows in the spectra of Figure 1, color-coordinated with the panel frames.

electrons as they traverse 200 nm of the material. Neglecting such a depletion, the theory for this case (Figure 1j) is dominated by a bulk mode, accompanied by symmetry-allowed surface modes. However, antisymmetric modes under inversion at the origin cannot be excited when the e-beam passes through the dimer center, which is the case of the low-energy dipolar mode.

Interestingly, the measured spectrum for the central trajectory in the nontouching dimer (Figure 1e, blue curve) shows (besides one of the surface modes observed for other beam locations) a high-energy feature that is slightly redshifted relative to the bulk plasmon, possibly contributed by partial penetration of the e-beam inside the material, as well as by the symmetric mode of the planar F-IO/vacuum/F-IO structure. Because the gap (g = 10 mm) is small compared to the cube side (200 nm), the structure can be assimilated to an infinite planar gap geometry, in which the electron can excite symmetric modes, whose electrostatic dispersion relation given by $[1 + \epsilon(\omega)]/[1 - \epsilon(\omega)] = \exp(-k_{\parallel}g)$ prescribes energies in the interval between the classical surface plasmon $\hbar\omega_{\rm p}/\sqrt{\epsilon_{\rm b}+1}\approx 0.65$ eV in the high-wave-vector limit $(k_{\parallel}g)$ \gg 1) and the bulk plasmon $\hbar\omega_{\rm p}/\sqrt{\epsilon_{\rm b}}\approx 0.73$ eV at $k_{\parallel}=0.$ The measured mode in this range is also reproduced by the corresponding numerical simulation (Figure 1j, blue curve).

The singular transition observed between touching and nontouching regimes in Figure 1 through the emergence of a mode in the former is in stark contrast to the transition when the cubes share a wider touching area, as shown in Figure 2 for a face-to-face configuration. The evolution of the spectra is smooth across the transition, as demonstrated by the simulations presented in Figure 2e–g. Also, experimental measurements (Figure 2a–c) confirm the absence of a low-energy feature for the touching configuration. Unfortunately, we could not find any narrow-gap nontouching face-to-face dimer, presumably because of the strong van der Waals attraction that pushes the faces toward collapse, as recently discussed in dielectric gaps with an exquisite degree of

control. Nonetheless, our level of confidence in the theory is supported by the excellent agreement that we find between the theory and the experiment for a wide range of nanocube configurations, including dissimilar dimers under touching and nearly touching conditions (Figures S6–S11 in Supporting Information), with geometrical parameters extracted from HAADF micrographs and dielectric properties modeled through the local dielectric function in eq 1. It should be noted that quantum confinement and nonlocal effects become relevant at small separations in the range of the Fermi wavelength of the material (e.g., $\lesssim 1$ nm in noble metals and F-ITO), leading to strong plasmon damping and frequency shifts $^{48-53}$ as well as emerging modes involving charge transfer via tunneling across the gap, 51,52 but we do not consider such small distances in the present work.

We note that the vertical scales in Figures 1 and 2 have absolute units (i.e., EELS probability per eV of energy loss range), which in the measured spectra are obtained by normalizing to the energy-integrated signal, including the zero-loss peak, except for Figure 1e, where part of the beam is always depleted by penetration through the material. The absolute magnitude of the EELS probability is in reasonably good agreement between the experiment (Figures 1b—d and 2a—c) and the theory (Figures 1g—i and 2e—g), although the spectral features in the theory are a bit narrower and higher, thus producing similar areas under the peaks.

Further insights into the nature of the plasmon modes in Figure 1 that illustrates a singular transition can be revealed by examining energy-filtered EELS maps at the corresponding peak energies in the spectra. We find that the measured maps are in excellent agreement with simulations for both touching and nontouching configurations, as shown in Figure 3. Incidentally, the cubes appear as black squares in the images due to e-beam depletion when passing through the material. The low-energy mode in the touching dimer (0.33 eV, Figure 3a,a') is confirmed to be absent in the nontouching dimer (Figure 3e,e'). In addition, the observed intensity pattern indicates an accumulation of charges at the opposite corners of

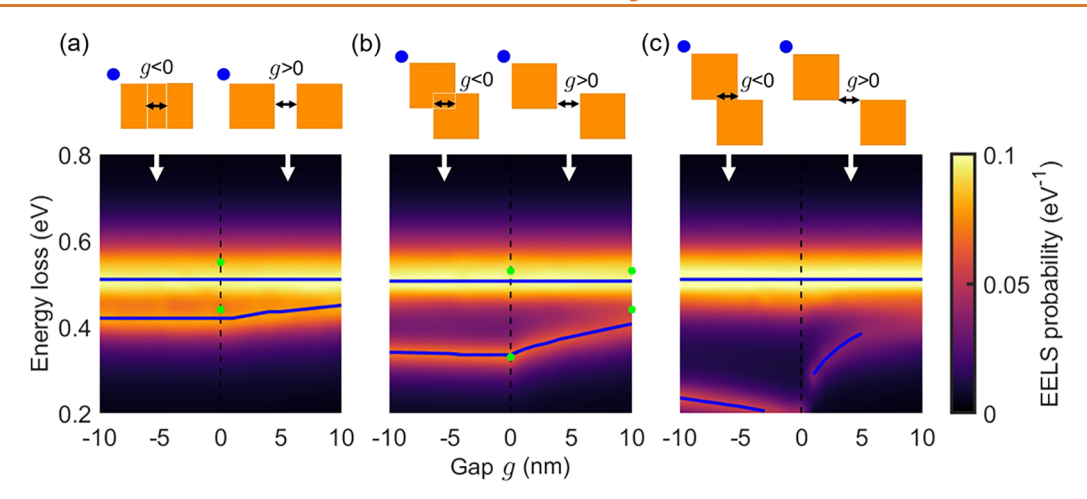


Figure 4. Touching-to-nontouching transition as a function of gap dimensionality for nanocube dimers. We show the EELS probability in the configurations shown in the upper sketches as a function of energy loss (vertical axis) and gap distance (horizontal axis; see sketches) for 60 keV electrons running perpendicular to the plane of representation and passing by the blue dots. Dimers are formed by F-IO nanocubes of 200 nm side length. Negative gaps indicate overlapping cubes. Panels (a,b) correspond to 2D touching regions defined by an entire cube face and one-third of a face, respectively, with green dots extracted from our experimental data. In panel (c), the cubes touch in a 1D region (an edge).

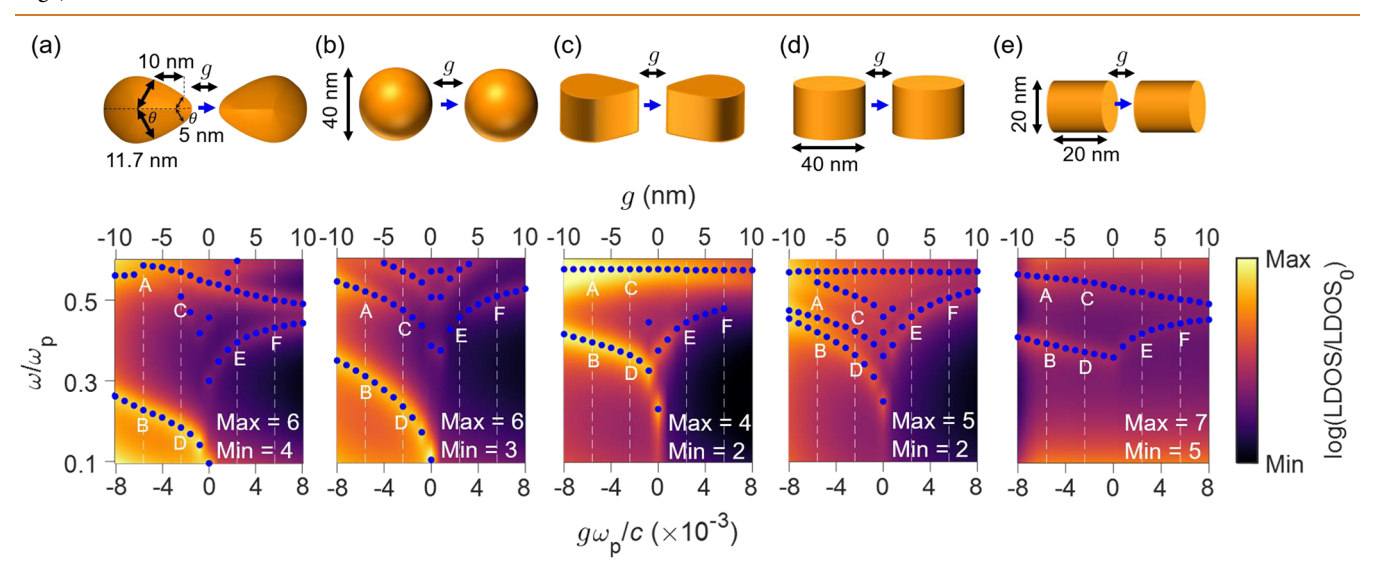


Figure 5. Touching-to-nontouching transition as a function of gap dimensionality for nanoparticles with different morphologies. We plot the LDOS at the gap center (projected on the direction across the gap) as a function of gap separation and photon energy for (a,b) zero-, (c,d) one-, and (e) two-dimensional touching regions. Blue-dotted curves are guides to the eye, indicating LDOS maxima. Different particle geometries are considered, as shown in the upper insets: (a) conical tips with a 11.7 nm spherical base radius, 5 nm tip rounding radius, 10 nm cone side length, and 60° cone angle; (b) 40 nm spheres; (c) side-by-side infinitely long wedge-like cylinders with the same transverse cross section as the particles in (a); (d) side-by-side infinitely long circular cylinders of 40 nm diameter; and (e) face-to-face finite cylinders of 20 nm diameter and 20 nm length. The material dielectric function is taken as $\varepsilon(\omega) = 1 - \omega_{\rm p}^{\ 2}/\omega(\omega + i\gamma)$ with $\gamma/\omega_{\rm p} = 0.05$. The upper horizontal scales indicate the gap distance for $\omega_{\rm p} = 1$ eV. In (c,d), the LDOS is expressed in momentum space $(q = \omega/\nu)$ for polarization along the gap direction with 60 keV electrons ($\nu \approx 0.446$ c) and normalized to $\omega/2\pi c^2$. In the rest of the plots, the real-space projected LDOS is normalized to the vacuum value LDOS₀ = $\omega^2/3\pi^2c^3$.

the nanocubes, revealing a dipolar mode that extends over the entire dimer. This interpretation is fully confirmed upon examination of the calculated surface-charge distributions associated with the peak spectral features in Figure 1g (insets).

When examining maps for filtered energies associated with the rest of the spectral features, both touching and non-touching regimes produce similar spatial patterns (cf. Figure 3b–d,f–h), therefore denoting the same charge ordering. More precisely, we observe additional modes dominated by edge (Figure 3b,f), face (Figure 3c,g), and bulk (Figure 3d,h) features, with similar intensity distributions apart from the gap

region. This interpretation is corroborated by the associated surface-charge distributions that we calculate for the spectral features in Figure 1h—j (insets).

Measured maps at the spectral features of the face-to-face touching configuration are presented in Figure S3 in Supporting Information, in excellent agreement with the theory. In addition, the latter shows minor modifications when the cubes are separated by a small 10 nm gap, therefore supporting the absence of a singular transition when the touching region is sufficiently large.

To analyze the dependence of the transition between touching and nontouching dimers on the dimensionality of the gap region, we consider F-IO nanocubes like those in Figures 1-3, but we introduce a lateral offset, as indicated in the upper insets of Figure 4. We then calculate the EELS probability for a fixed position of the electron and plot the result as a function of lost energy and gap separation (color plots in Figure 4). Negative gaps correspond to physically overlapping particles. We note that the highest-energy spectral feature remains at a nearly constant energy of 0.51 eV for all configurations and gap distances, thus indicating that this is a corner mode similar to that of the individual nanocube (see Figures S1 and S2 in Supporting Information). In contrast, the lowest-energy spectral peak undergoes substantial variations with the gap distance and also displays a strong dependence on the lateral offset. For touching dimers, this mode exhibits a mild dependence on overlap (i.e., negative gap distance), while its energy redshifts with increasing offset (from Figure 4a-c) as expected for more elongated metallic structures.⁵⁴ Without offset (Figure 4a, a configuration previously investigated in gold cube dimers⁴³), the mode is continued without interruption at a similar energy after a gap is introduced and eventually blue shifts as the separation increases. In contrast, an abrupt discontinuity is observed for large offsets if the touching point is just an edge (Figure 4c), indicating a variation in the nature of the mode. In the nontouching dimer, induced charges of opposite signs increasingly accumulate near the gap region as the separation is reduced, thus producing an attractive capacitive interaction that redshifts the low-energy plasmon. 43 These results are consistent with those observed in the analysis of Figures 1-3.

The touching-to-nontouching transition thus depends on the dimensionality of the touching area (two-dimensional (2D) in Figure 4a,b and one-dimensional (1D) in Figure 4c). To better understand the nature of this dependence, we analyze dimer geometries featuring zero-dimensional (0D), 1D, and 2D gaps in Figure 5a,b (point-to-point tips and spheres), Figure 5c,d (edge-to-edge infinite, translationally invariant geometries), and Figure 5e (face-to-face finite cylinders), respectively, which extends previous analyses for rod dimers with rounded and flat edges;³⁰ sphere-cube dimers;⁵⁵ and sphere, disk, and cube dimers.⁵⁶ Incidentally, overlapping particles are characterized in general by sharp edges at the junctions, which can produce a singular behavior, 57 so we smooth them by introducing a small rounding radius. We then calculate the local density of optical states (LDOS) at a point placed in the center of the structure (see Methods). The LDOS is defined as the sum of the normalized electric-field intensities associated with all optical modes as a function of frequency, position, and field direction.^{58,59} We take the latter across the gap in our calculations (see the blue arrows in the upper insets of Figure 5). Then, the maxima of the LDOS in the plots of Figure 5 correspond to localized modes, which we highlight by superimposing blue-dotted curves as guides to the eye. We observe that 0D and 1D touching regions (Figure 5a-d) lead to a singular transition characterized by the sudden disappearance of the lowest-energy mode present in the touching dimers (involving net charges in each of the particles²⁹) as soon as the particles are separated. This is in contrast to 2D regions (Figure 5e), which produce a smooth transition. The induced charge densities associated with the observed modes (Figure S4 in Supporting Information)

corroborate this picture and further support the smooth transition occurring with 2D touching regions. Incidentally, under external illumination, these structures produce a large optical electric-field amplification at the gap of nontouching dimers for frequencies roughly in agreement with those of the LDOS peaks (see Figure S5 in Supporting Information), and we find that higher values of the near-field enhancement are reached when approaching the touching transition in 0D gap geometries (Figure S5a,b). The results portrayed in Figures 5 and S5 assume a Drude dielectric function (eq 1 with $\epsilon_{\rm b}=1$), but a similar behavior is observed for gold and silver (see Figures S12–S15 in Supporting Information), although the singular character of the transition is less clear for 1D gaps due to higher losses in this material.

CONCLUSIONS

In summary, our experimental and theoretical investigation of fluorine-doped indium-oxide nanocube dimers reveals a dramatic variation of their infrared plasmons with particle distance and lateral offset, allowing us to explore the transition between touching and nontouching regimes and find evidence of different behavior depending on the dimensionality of the touching area. By further examining a representative range of both nanoparticle and gap morphologies, we conclude that the transition is singular for point- and line-like touching regions, characterized by a low-energy dipolar plasmon in which a netinduced charge is present in each of the particles. On the touching side, the low-energy mode evolves toward increasingly low frequencies near the touching region. This mode disappears as soon as the particles are separated. In contrast, for 2D touching regions, the transition is smooth, featuring a low-energy mode with a continuous evolution of frequency, which reaches a minimum under just-touching conditions. Our results provide valuable information on the role of narrow gaps in plasmonic structures, commonly used in applications requiring optical sensing and nonlinear enhancement at the nanoscale.

METHODS

Materials. Indium(III) acetylacetonate [In(acac)₃, 99.99%], Indium(III) fluoride (InF₃, >99.9%), Oleic acid (OA, 90%, technical grade), Octylamine (OcAm, 99%), and Trioctylamine (TOA, 98%) were purchased from Sigma-Aldrich. Toluene (99.5%) was purchased from Fisher Chemical. All chemicals were used as received without any further purification.

Fluorine-Doped Indium Oxide (F-IO) Nanocube Synthesis. All synthesis procedures were carried out using standard Schlenk line techniques aided by a nitrogen-filled glovebox. 35 For the growth of F/ In₂O₃ cubes (F-IO), a mixture of In(acac)₃ (399.78 mg, 0.97 mmol), InF₃ (5.15 mg, 0.03 mmol), OA (1 mL), OcAm (0.5 mL), and TOA (3.5 mL) was loaded in a three-neck round-bottom flask in the glovebox. This precursor mixture was then stirred with a magnetic bar at 600 rpm and degassed under vacuum at 120 °C for 15 min. The mixture turned transparent during this operation. Thereafter, the flask was filled with nitrogen and further heated at a ramp rate of 15 °C/ min to 320 °C. The reaction mixture turned opaque, which indicated cube growth. The reaction was allowed to run for 5 min at 320 °C. Subsequently, growth was terminated by removing the heating mantle. The cubes were purified to remove excess OA ligand surfactants by dispersing the solution in toluene and centrifuging at 4500 rpm for 5 min until a solid pellet formed at the bottom of the centrifuge tube. The supernatant was disposed of, and the solid pellet was redispersed in toluene. This purification process was repeated three times. The resultant cubes were redispersed in toluene for further analysis. Samples were prepared by dropcasting diluted 0.01

mg/mL nanocube dispersions onto thin (25 nm) silicon nitride TEM grids (Ted Pella). Surface organic ligands were removed from the TEM grid samples after dropcast loading using plasma cleaning in Ar for 15 min, in addition to heating under vacuum at $120-160\,^{\circ}\text{C}$.

Monochromated EELS Measurements. EELS data sets were acquired on a Nion high-energy-resolution monochromated EELS scanning transmission electron microscope (STEM) (HERMES) operated at 60 kV equipped with a Nion Iris spectrometer and a Hamamatsu ORCA SCMOS detector. An energy resolution of ∼12 meV, as determined by the full width at half maximum of the elastic scattering (or zero loss) peak, was selected as an optimum balance of reducing background while maintaining a reasonable beam current. The dipole mode of the touching nanoparticle system was measured to have a width of 85 meV, indicating that the energy resolution itself did not contribute to the line width of the peaks. Particles selected for EELS analysis were deposited on silicone-nitride membranes (25 nm thickness) and were selected by searching for particles with similar orientations but different gaps.

EELS Simulations. We calculate the EELS probability $\Gamma_{\rm EELS}(\omega)$ as a function of energy loss $\hbar\omega$ by using the well-known expression ⁶⁰

$$\Gamma_{\text{EELS}}(\mathbf{R}_0, \, \omega) = \frac{e}{\pi \hbar \omega} \int dz \, \operatorname{Re} \{ e^{-i\omega z/\nu} E_z^{\text{ind}}(\mathbf{R}_0, \, z, \, \omega) \}$$
 (2)

where the electron is assumed without loss of generality to move along z with velocity ν and pass through the transverse position \mathbf{R}_0 = (x_0, y_0) . The EELS probability is normalized such that $\int_0^\infty \hbar \omega \ d\omega$ $\Gamma_{\text{EELS}}(\mathbf{R}_0,\omega)$ is the average energy loss experienced by the electron. For geometries involving cubes (Figures 1-4, and S1-S3), we calculate the field $\mathbf{E}^{\text{ind}}(\mathbf{r}, \omega)$ induced by the passage of the electron in the frequency domain through a finite-element method (COMSOL) in which the electron is introduced as a line current source $\mathbf{j}(\mathbf{r}, \omega) = -e\delta(\mathbf{R} - \mathbf{R}_0)e^{i\omega z/v}\hat{\mathbf{z}}$. For axially symmetric (Figures 5a,b,e, S4a,b,e, and S5a,b,e) and translationally invariant (Figures 5c,d, S4c,d, and S5c,d) geometries, we use the boundary-element method (BEM), as detailed elsewhere.⁶¹ In all cases, we model the materials through the modified Drude dielectric function given in eq 1. Figures 1–4 and S1–S3 are obtained with dielectric parameters $\epsilon_{\rm b}$ = 4, $\hbar\omega_{\rm p}$ = 1.46 eV, and $\hbar\gamma$ = 0.07 eV, where we modify $\omega_{\rm p}$ (but maintain $\epsilon_{\rm b}$ and γ) relative to the previously reported optical data for F-IO³⁵ to accommodate the actual level of doping in our samples and obtain the best fit to experiments. Slightly different parameters are taken in Figures 5, S4, S5, and S12-S15 to better visualize the neartouching transition for generic Drude particles, as well as for gold and silver.

LDOS Simulations. For the finite structures in Figure 5a,b,e, we calculate the LDOS at a position \mathbf{r} at the gap center, projected on a direction $\hat{\mathbf{n}}$ across the gap, as 59,62,63

$$\rho_{\hat{\mathbf{n}}}(\mathbf{r}, \omega) = \rho_{\hat{\mathbf{n}}}^{0}(\omega) + (2\pi^{2}\omega)^{-1} \operatorname{Im}\{\hat{\mathbf{n}} \cdot \mathbf{E}^{\operatorname{ind}}(\mathbf{r})\}$$

where $\rho_{\hat{\mathbf{n}}}^{0}(\omega) = \omega^{2}/3\pi^{2}c^{3}$ is the LDOS in free space, while the second term is the imaginary part of the electric field that is self-induced by a unit point dipole directed along $\hat{\mathbf{n}}$ and placed at \mathbf{r} . We obtained the induced field using either COMSOL for cube dimers or BEM for the rest of the structures. For translationally invariant geometries (Figure 5c,d), we express the LDOS in momentum space q along $\hat{\mathbf{n}}$. Note that we use a different normalization of the LDOS in Figure 5 for finite structures and for translational invariant geometries to accommodate the differences in their definitions.

ASSOCIATED CONTENT

5 Supporting Information

The Supporting Information is available free of charge at https://pubs.acs.org/doi/10.1021/acsnano.4c02644.

Analysis and energy-filtered plasmon EELS spectra and maps of an individual F-IO nanocube (Figures S1 and S2); energy-filtered plasmon EELS maps in face-to-face touching and nontouching nanocube dimers (Figure

S3); induced surface charges associated with the spectral features (Figure S4); field enhancement under the same conditions (Figure S5); analysis and energy-filtered plasmon EELS maps of nearly touching F-IO nanocubes with two different sizes (Figure S6 and S7); analysis and energy-filtered plasmon EELS maps of touching F-IO nanocubes with two different sizes (Figure S8 and S9); analysis and energy-filtered plasmon EELS maps of three touching F-IO nanocubes (Figure S10 and S11); touching-to-nontouching transition for gold and silver nanoparticles under the same geometrical configurations as in Figure 5 (Figure S12 and S13); field enhancement under the same geometrical conditions for nontouching gold and silver dimers (Figure S14 and S15); and effect of the TEM sample membrane (Figure S16) (PDF)

AUTHOR INFORMATION

Corresponding Authors

Jordan A. Hachtel — Center for Nanophase Materials Sciences, Oak Ridge National Laboratory, Oak Ridge, Tennessee 37831, United States; Occid.org/0000-0002-9728-0920; Email: hachtelja@ornl.gov

F. Javier García de Abajo — the Barcelona Institute of Science and Technology, ICFO-Institut de Ciencies Fotoniques, Barcelona 08860, Spain; ICREA-Institució Catalana de Recerca i Estudis Avançats, Barcelona 08010, Spain; orcid.org/0000-0002-4970-4565;

Email: javier.garciadeabajo@nanophotonics.es

Authors

Yina Wu − the Barcelona Institute of Science and Technology, ICFO-Institut de Ciencies Fotoniques, Barcelona 08860, Spain; ocid.org/0000-0001-8895-4156

Andrea Konečná – the Barcelona Institute of Science and Technology, ICFO-Institut de Ciencies Fotoniques, Barcelona 08860, Spain; Central European Institute of Technology, Brno University of Technology, Brno 61200, Czech Republic; Institute of Physical Engineering, Brno University of Technology, Brno 61669, Czech Republic; orcid.org/0000-0002-7423-5481

Shin Hum Cho – Department of Chemical Engineering, Keimyung University, Daegu 42601, Republic of Korea; orcid.org/0000-0002-0271-116X

Delia J. Milliron – McKetta Department of Chemical Engineering, the University of Texas at Austin, Austin, Texas 78712, United States; orcid.org/0000-0002-8737-451X

Complete contact information is available at: https://pubs.acs.org/10.1021/acsnano.4c02644

Notes

The authors declare no competing financial interest.

ACKNOWLEDGMENTS

This work has been supported in part by the European Research Council (Advanced grant 789104-eNANO), the European Commission (Horizon 2020 grants 101017720 FET-Proactive EBEAM and 964591-SMART-electron), the Spanish MICINN (PID2020-112625GB-I00 and Severo Ochoa CEX2019-000910-S), the Catalan CERCA Program, Fundaciós Cellex and Mir-Puig, the Czech Science Foundation (Junior Star grant no. 23-05119M), and a 2024 Bisa Research Grant by Keimyung University. Nanocrystal synthesis and

characterization were supported by the Welch Foundation (F-1848) and National Science Foundation (CHE-2303296). STEM and EELS experiments were supported by the Center for Nanophase Materials Sciences (CNMS, a U.S. Department of Energy, Office of Science User Facility), conducted using instrumentation within ORNL's Materials Characterization Core provided by UT-Batelle, LLC, under contract no. DE-AC05-00OR22725 with the U.S. Department of Energy, sponsored by the Laboratory Directed Research and Development Program of ORNL.

REFERENCES

- (1) Kreibig, U.; Vollmer, M. Optical Properties of Metal Clusters; Springer-Verlag: Berlin, 1995.
- (2) Wang, L.; Hasanzadeh Kafshgari, M.; Meunier, M. Optical Properties and Applications of Plasmonic-Metal Nanoparticles. *Adv. Funct. Mater.* **2020**, *30*, 2005400.
- (3) Gonçalves, P. A. D. Plasmonics and Light-Matter Interactions in Two-Dimensional Materials and in Metal Nanostructures: Classical and Quantum Considerations; Springer Nature: Switzerland, 2020.
- (4) Hodak, J. H.; Martini, I.; Hartland, G. V. Spectroscopy and Dynamics of Nanometer-Sized Noble Metal Particles. *J. Phys. Chem. B* **1998**, *102*, 6958–6967.
- (5) Kim, S.; Kim, J.-M.; Park, J.-E.; Nam, J.-M. Nonnoble-Metal-Based Plasmonic Nanomaterials: Recent Advances and Future Perspectives. *Adv. Mater.* **2018**, *30*, 1704528.
- (6) Min, C.; Shen, Z.; Shen, J.; Zhang, Y.; Fang, H.; Yuan, G.; Du, L.; Zhu, S.; Lei, T.; Yuan, X. Focused Plasmonic Trapping of Metallic Particles. *Nat. Commun.* **2013**, *4*, 2891.
- (7) Nordlander, P.; Oubre, C.; Prodan, E.; Li, K.; Stockman, M. I. Plasmon Hybridization in Nanoparticle Dimers. *Nano Lett.* **2004**, *4*, 899–903.
- (8) Gunnarsson, L.; Rindzevicius, T.; Prikulis, J.; Kasemo, B.; Käll, M.; Zou, S.; Schatz, G. C. Confined Plasmons in Nanofabricated Single Silver Particle Pairs: Experimental Observations of Strong Interparticle Interactions. *J. Phys. Chem. B* **2005**, *109*, 1079–1087.
- (9) Jain, P. K.; Huang, W.; El-Sayed, M. A. On the Universal Scaling Behavior of the Distance Decay of Plasmon Coupling in Metal Nanoparticle Pairs: A Plasmon Ruler Equation. *Nano Lett.* **2007**, *7*, 2080–2088.
- (10) Halas, N. J.; Lal, S.; Chang, W.; Link, S.; Nordlander, P. Plasmons in Strongly Coupled Metallic Nanostructures. *Chem. Rev.* **2011**, *111*, 3913–3961.
- (11) Ren, Y.; Qi, H.; Chen, Q.; Wang, S.; Ruan, L. Localized Surface Plasmon Resonance of Nanotriangle Dimers at Different Relative Positions. J. Quant. Spectrosc. Radiat. 2017, 199, 45–51.
- (12) Aćimović, S. S.; Kreuzer, M. P.; González, M. U.; Quidant, R. Plasmon Near-Field Coupling in Metal Dimers as a Step Toward Single-Molecule Sensing. ACS Nano 2009, 3, 1231–1237.
- (13) Göeken, K. L.; Subramaniam, V.; Gill, R. Enhancing Spectral Shifts of Plasmon-Coupled Noble Metal Nanoparticles for Sensing Applications. *Phys. Chem. Chem. Phys.* **2015**, *17*, 422–427.
- (14) Wang, H.; Liu, T.; Huang, Y.; Fang, Y.; Liu, R.; Wang, S.; Wen, W.; Sun, M. Plasmon-Driven Surface Catalysis in Hybridized Plasmonic Gap Modes. *Sci. Rep.* **2014**, *4*, 7087.
- (15) Wang, Y.; Fang, L.; Gong, M.; Deng, Z. Chemically Modified Nanofoci Unifying Plasmonics and Catalysis. *Chem. Sci.* **2019**, *10*, 5929–5934.
- (16) Lei, D. Y.; Aubry, A.; Luo, Y.; Maier, S. A.; Pendry, J. B. Plasmonic Interaction between Overlapping Nanowires. *ACS Nano* **2011**, *5*, 597–607.
- (17) Nehl, C. L.; Liao, H.; Hafner, J. H. Optical Properties of Star-Shaped Gold Nanoparticles. *Nano Lett.* **2006**, *6*, 683–688.
- (18) Xu, H.; Aizpurua, J.; Käll, M.; Apell, P. Electromagnetic Contributions to Single-Molecule Sensitivity in Surface-Enhanced Raman Scattering. *Phys. Rev. E* **2000**, *62*, 4318–4324.
- (19) Sun, Y.; Xia, Y. Shape-Controlled Synthesis of Gold and Silver Nanoparticles. *Science* **2002**, 298, 2176–2179.

- (20) Hayazawa, N.; Inouye, Y.; Sekkat, Z.; Kawata, S. Metallized Tip Amplification of Near-Field Raman Scattering. *Opt. Commun.* **2000**, *183*, 333–336.
- (21) Lalayan, A. A.; Bagdasaryan, K. S.; Petrosyan, P. G.; Nerkararyan, K. V.; Ketterson, J. B. Anomalous Field Enhancement from Superfocusing of Surface Plasmons at Contacting Silver Surfaces. *J. Appl. Phys.* **2002**, *91*, 2965–2968.
- (22) Katyal, J. Plasmonic Coupling in Au, Ag and Al Nanosphere Homo-Dimers for Sensing and SERS. *Adv. Electromagn.* **2018**, *7*, 83–90
- (23) Murphy, C. J.; Sau, T. K.; Gole, A.; Orendorff, C. J. Surfactant-Directed Synthesis and Optical Properties of One-Dimensional Plasmonic Metallic Nanostructures. *MRS Bull.* **2005**, *30*, 349–355.
- (24) Lassiter, J. B.; Aizpurua, J.; Hernandez, L. I.; Brandl, D. W.; Romero, I.; Lal, S.; Hafner, J. H.; Nordlander, P.; Halas, N. J. Close Encounters between Two Nanoshells. *Nano Lett.* **2008**, *8*, 1212–1218.
- (25) Oldenburg, S.; Averitt, R.; Westcott, S.; Halas, N. Nanoengineering of Optical Resonances. *Chem. Phys. Lett.* **1998**, 288, 243–247
- (26) Willets, K. A.; Van Duyne, R. P. Localized Surface Plasmon Resonance Spectroscopy and Sensing. *Annu. Rev. Phys. Chem.* **2007**, 58, 267–297.
- (27) Zheng, P.; Tang, H.; Liu, B.; Kasani, S.; Huang, L.; Wu, N. Origin of Strong and Narrow Localized Surface Plasmon Resonance of Copper Nanocubes. *Nano Res.* **2019**, *12*, 63–68.
- (28) Prodan, E.; Radloff, C.; Halas, N. J.; Nordlander, P. A Hybridization Model for the Plasmon Response of Complex Nanostructures. *Science* **2003**, 302, 419–422.
- (29) Romero, I.; Aizpurua, J.; Bryant, G. W.; García De Abajo, F. J. Plasmons in Nearly Touching Metallic Nanoparticles: Singular Response in the Limit of Touching Dimers. *Opt. Express* **2006**, *14*, 9988–9999.
- (30) Esteban, R.; Aguirregabiria, G.; Borisov, A. G.; Wang, Y. M.; Nordlander, P.; Bryant, G. W.; Aizpurua, J. Morphology of Narrow Gaps Modifies the Plasmonic Response. *ACS Photonics* **2015**, *2*, 295–305.
- (31) Atay, T.; Song, J. H.; Nurmikko, A. V. Strongly Interacting Plasmon Nanoparticle Pairs: From Dipole-Dipole Interaction to Conductively Coupled Regime. *Nano Lett.* **2004**, *4*, 1627–1631.
- (32) Slaughter, L. S.; Wu, Y.; Willingham, B. A.; Nordlander, P.; Link, S. Effects of Symmetry Breaking and Conductive Contact on the Plasmon Coupling in Gold Nanorod Dimers. *ACS Nano* **2010**, *4*, 4657–4666.
- (33) Tan, S. F.; Wu, L.; Yang, J. K.; Bai, P.; Bosman, M.; Nijhuis, C. A. Quantum Plasmon Resonances Controlled by Molecular Tunnel Junctions. *Science* **2014**, *343*, 1496–1499.
- (34) Knebl, D.; Hörl, A.; Trügler, A.; Kern, J.; Krenn, J. R.; Puschnig, P.; Hohenester, U. Gap Plasmonics of Silver Nanocube Dimers. *Phys. Rev. B* **2016**, *93*, 081405.
- (35) Cho, S. H.; Ghosh, S.; Berkson, Z. J.; Hachtel, J. A.; Shi, J.; Zhao, X.; Reimnitz, L. C.; Dahlman, C. J.; Ho, Y.; Yang, A.; Liu, Y.; Idrobo, J.-C.; Chmelka, B. F.; Milliron, D. J. Syntheses of Colloidal F: In₂O₃ Cubes: Fluorine-Induced Faceting and Infrared Plasmonic Response. *Chem. Mater.* **2019**, *31*, 2661–2676.
- (36) Cho, S. H.; Roccapriore, K. M.; Dass, C. K.; Ghosh, S.; Choi, J.; Noh, J.; Reimnitz, L. C.; Heo, S.; Kim, K.; Xie, K.; Korgel, B. A.; Li, X.; Hendrickson, J. R.; Hachtel, J. A.; Milliron, D. J. Spectrally Tunable Infrared Plasmonic F,Sn:In₂O₃ Nanocrystal Cubes. *J. Chem. Phys.* **2020**, *152*, 014709.
- (37) Kalusniak, S.; Sadofev, S.; Henneberger, F. ZnO as a Tunable Metal: New Types of Surface Plasmon Polaritons. *Phys. Rev. Lett.* **2014**, *112*, 137401.
- (38) Genç, A.; Patarroyo, J.; Sancho-Parramon, J.; Arenal, R.; Duchamp, M.; Gonzalez, E. E.; Henrard, L.; Bastús, N. G.; Dunin-Borkowski, R. E.; Puntes, V. F.; Arbiol, J. Tuning the Plasmonic Response Up: Hollow Cuboid Metal Nanostructures. *ACS Photonics* **2016**, *3*, 770–779.

- (39) Lounis, S. D.; Runnerstrom, E. L.; Llordes, A.; Milliron, D. J. Defect Chemistry and Plasmon Physics of Colloidal Metal Oxide Nanocrystals. *J. Phys. Chem. Lett.* **2014**, *5*, 1564–1574.
- (40) Liu, Y.; Liu, M.; Swihart, M. T. Plasmonic Copper Sulfide-Based Materials: A Brief Introduction to Their Synthesis, Doping, Alloying, and Applications. *J. Phys. Chem. C* **2017**, *121*, 13435–13447.
- (41) Schimpf, A. M.; Knowles, K. E.; Carroll, G. M.; Gamelin, D. R. Electronic Doping and Redox-Potential Tuning in Colloidal Semi-conductor Nanocrystals. *Acc. Chem. Res.* **2015**, *48*, 1929–1937.
- (42) Runnerstrom, E. L.; Llordés, A.; Lounis, S. D.; Milliron, D. J. Nanostructured Electrochromic Smart Windows: Traditional Materials and NIR-Selective Plasmonic Nanocrystals. *Chem. Commun.* **2014**, *50*, 10555–10572.
- (43) Kim, D.-S.; Heo, J.; Ahn, S.-H.; Han, S. W.; Yun, W. S.; Kim, Z. H. Real-Space Mapping of the Strongly Coupled Plasmons of Nanoparticle Dimers. *Nano Lett.* **2009**, *9*, 3619–3625.
- (44) Fuchs, R. Theory of the Optical Properties of Small Cubes. *Phys. Lett.* **1974**, 48, 353–354.
- (45) Fuchs, R. Theory of the Optical Properties of Ionic Crystal Cubes. *Phys. Rev. B: Solid State* 1975, 11, 1732–1740.
- (46) McMahon, J. M.; Wang, Y.; Sherry, L. J.; Van Duyne, R. P.; Marks, L. D.; Gray, S. K.; Schatz, G. C. Correlating the Structure, Optical Spectra, and Electrodynamics of Single Silver Nanocubes. *J. Phys. C* **2009**, *113*, 2731–2735.
- (47) Babar, A. N.; Weis, T. A. S.; Tsoukalas, K.; Kadkhodazadeh, S.; Arregui, G.; Vosoughi Lahijani, B.; Stobbe, S. Self-Assembled Photonic Cavities with Atomic-Scale Confinement. *Nature* **2023**, 624, 57–63.
- (48) Liebsch, A. Surface-Plasmon Dispersion and Size Dependence of Mie Resonance: Silver Versus Simple Metals. *Phys. Rev. B: Condens. Matter Mater. Phys.* **1993**, 48, 11317–11328.
- (49) García de Abajo, F. J. Nonlocal Effects in the Plasmons of Strongly Interacting Nanoparticles, Dimers, and Waveguides. *J. Phys. Chem. C* **2008**, *112*, 17983–17987.
- (50) Zuloaga, J.; Prodan, E.; Nordlander, P. Quantum Description of the Plasmon Resonances of a Nanoparticle Dimer. *Nano Lett.* **2009**, *9*, 887–891.
- (51) Esteban, R.; Borisov, A. G.; Nordlander, P.; Aizpurua, J. Bridging Quantum and Classical Plasmonics with a Quantum-Corrected Model. *Nat. Commun.* **2012**, *3*, 825.
- (52) Savage, K. J.; Hawkeye, M. M.; Esteban, R.; Borisov, A. G.; Aizpurua, J.; Baumberg, J. J. Revealing the Quantum Regime in Tunnelling Plasmonics. *Nature* **2012**, *491*, 574–577.
- (53) Cha, H.; Yoon, J. H.; Yoon, S. Probing Quantum Plasmon Coupling Using Gold Nanoparticle Dimers with Tunable Interparticle Distances down to the Subnanometer Range. *ACS Nano* **2014**, *8*, 8554–8563.
- (54) Myroshnychenko, V.; Rodríguez-Fernández, J.; Pastoriza-Santos, I.; Funston, A. M.; Novo, C.; Mulvaney, P.; Liz-Marzán, L. M.; García de Abajo, F. J. Modelling the Optical Response of Gold Nanoparticles. *Chem. Soc. Rev.* **2008**, *37*, 1792–1805.
- (55) Kim, M.; Kwon, H.; Lee, S.; Yoon, S. Effect of Nanogap Morphology on Plasmon Coupling. ACS Nano 2019, 13, 12100–12108.
- (56) Devaraj, V.; Lee, J.-M.; Kim, Y.-J.; Jeong, H.; Oh, J.-W. Engineering Efficient Self-Assembled Plasmonic Nanostructures by Configuring Metallic Nanoparticle's Morphology. *Int. J. Mol. Sci.* **2021**, 22, 10595.
- (57) Davis, L. C. Electostatic edge modes of a dielectric wedge. *Phys. Rev. B: Solid State* **1976**, *14*, 5523–5525.
- (58) Fussell, D. P.; McPhedran, R. C.; Martijn de Sterke, C. Three-Dimensional Green's Tensor, Local Density of States, and Spontaneous Emission in Finite Two-Dimensional Photonic Crystals Composed of Cylinders. *Phys. Rev. E* **2004**, *70*, 066608.
- (59) García de Abajo, F. J.; Kociak, M. Probing the Photonic Local Density of States with Electron Energy Loss Spectroscopy. *Phys. Rev. Lett.* **2008**, *100*, 106804.
- (60) García de Abajo, F. J. Optical Excitations in Electron Microscopy. *Rev. Mod. Phys.* **2010**, 82, 209–275.

- (61) García de Abajo, F. J.; Howie, A. Retarded Field Calculation of Electron Energy Loss in Inhomogeneous Dielectrics. *Phys. Rev. B: Condens. Matter Mater. Phys.* **2002**, *65*, 115418.
- (62) Blanco, L. A.; García de Abajo, F. J. Spontaneous Light Emission in Complex Nanostructures. *Phys. Rev. B: Condens. Matter Mater. Phys.* **2004**, *69*, 205414.
- (63) Novotny, L.; Hecht, B. *Principles of Nano-Optics*; Cambridge University Press: New York, 2006.